Supplemental material for "Topological properties of a dense atomic lattice gas"

Robert J. Bettles,[1] Jiří Minář,[2,3] Charles S. Adams,[1] Igor Lesanovsky,[2,3] and Beatriz Olmos[2,3,*]

[1] *Joint Quantum Center (JQC) Durham-Newcastle, Department of Physics, Durham University, South Road, Durham DH1 3LE, United Kingdom*
[2] *School of Physics and Astronomy, The University of Nottingham, Nottingham, NG7 2RD, United Kingdom*
[3] *Centre for the Mathematics and Theoretical Physics of Quantum Non-equilibrium Systems, The University of Nottingham, Nottingham, NG7 2RD, UK*

In this Supplemental Material, we provide the derivation of the master equation that describes the dynamics of our system. Next, we show how to perform the Ewald summation for the calculation of the band structure, including details of its numerical implementation. Finally, we discuss the impact of the finite-size of the system on the topological properties, the edge states and the nature of the bulk-boundary relation.

* beatriz.olmos-sanchez@nottingham.ac.uk

I. COUPLING TO THE MULTIMODE RADIATION FIELD

The atomic system is coupled to the quantized multimode radiation field. Within the dipole approximation, the Hamiltonian that describes the dynamics of the atomic ensemble and the radiation field reads

$$H_{\rm af} = \sum_{j=1}^{N} \hbar\omega_{\rm a} \mathbf{b}_j^\dagger \cdot \mathbf{b}_j + \sum_{\mathbf{q}\lambda} \hbar\omega_{\mathbf{q}} a_{\mathbf{q}\lambda}^\dagger a_{\mathbf{q}\lambda} + i\hbar \sum_{j=1}^{N} \sum_{\mathbf{q}\lambda} \mathbf{g}_{\mathbf{q}\lambda} \cdot \left(a_{\mathbf{q}\lambda}^\dagger \mathbf{s}_j e^{-i\mathbf{q}\cdot\mathbf{r}_j} - \mathbf{s}_j a_{\mathbf{q}\lambda} e^{i\mathbf{q}\cdot\mathbf{r}_j} \right). \tag{S1}$$

The first term represents the atomic energy, with $\hbar\omega_{\rm a} = 2\pi\hbar c/\lambda$ being the energy difference between the ground ($|g\rangle$) and the three degenerate $J = 1$ manifold states ($|-\rangle$, $|0\rangle$ and $|+\rangle$ for $m_J = -1, 0$ and $+1$, respectively) and the vector transition operator for the j-th atom (located at $\mathbf{r}_j$) being defined as $\mathbf{b}_j = \left(|g\rangle_j\langle +|, |g\rangle_j\langle -|, |g\rangle_j\langle 0| \right)^T$. The second term of the Hamiltonian represents the radiation field, and here $\hbar\omega_{\mathbf{q}}$ is the energy of a photon with momentum $\mathbf{q}$ and polarization λ and $a_{\mathbf{q}\lambda}$ is the annihilation operator of such a photon ($[a_{\mathbf{q}\lambda}, a_{\mathbf{q}'\lambda'}^\dagger] = \delta_{\mathbf{q}\mathbf{q}'}\delta_{\lambda\lambda'}$). The last term represents the coupling between the two systems, with $\mathbf{s}_j = \mathbf{b}_j^\dagger + \mathbf{b}_j$ and the coupling coefficient being given by $\mathbf{g}_{\mathbf{q}\lambda} = d\sqrt{\frac{\omega_{\mathbf{q}}}{2\epsilon_0\hbar V}}\hat{e}_{\mathbf{q}\lambda}$, where V is the quantization volume, d the modulus of the transition dipole moment between the ground and the three degenerate excited states, and $\hat{e}_{\mathbf{q}\lambda}$ the unit polarization vector of the photon ($\mathbf{q}\cdot\hat{e}_{\mathbf{q}\lambda} = 0$).

Within the dipole and Born-Markov approximations, and tracing out the environment, one obtains the quantum master equation for the atomic density matrix ρ,

$$\dot{\rho} = -\frac{i}{\hbar}\left[H, \rho\right] + \mathcal{D}(\rho), \tag{S2}$$

which describes the dynamics of the atomic degrees of freedom [1–3]. The many-body Hamiltonian that describes the coherent evolution of the system reads

$$H = \hbar \sum_{j\neq l} \mathbf{b}_j^\dagger \cdot \overline{W}_{jl} \cdot \mathbf{b}_l, \tag{S3}$$

characterized by the coefficient matrix (assuming all atoms localized on the xy-plane)

$$\overline{W}_{jl} = \begin{pmatrix} A_{jl} & B_{jl}e^{-2i\phi_{jl}} & 0 \\ B_{jl}e^{2i\phi_{jl}} & A_{jl} & 0 \\ 0 & 0 & C_{jl} \end{pmatrix} \tag{S4}$$

with A_{jl} and B_{jl} being defined in the main text [Eqs. (6) and (7), respectively] and

$$C_{jl} = \frac{3\Gamma}{4}\left[-\frac{\cos\kappa_{jl}}{\kappa_{jl}} + \frac{\sin\kappa_{jl}}{\kappa_{jl}^2} + \frac{\cos\kappa_{jl}}{\kappa_{jl}^3} \right] \tag{S5}$$

for $j \neq l$. The dissipator $\mathcal{D}(\rho)$ reads

$$\mathcal{D}(\rho) = \sum_{jl} \mathbf{b}_j \cdot \overline{\Gamma}_{jl} \cdot \rho \mathbf{b}_l^\dagger - \frac{1}{2}\left\{ \mathbf{b}_j^\dagger \cdot \overline{\Gamma}_{jl} \cdot \mathbf{b}_l, \rho \right\}, \tag{S6}$$

where

$$\overline{\Gamma}_{jl} = \begin{pmatrix} A'_{jl} & B'_{jl}e^{-2i\phi_{jl}} & 0 \\ B'_{jl}e^{2i\phi_{jl}} & A'_{jl} & 0 \\ 0 & 0 & C'_{jl} \end{pmatrix}, \tag{S7}$$

with A'_{jl} and B'_{jl} being defined in the main text [Eqs. (8) and (9), respectively] and

$$C'_{jl} = \frac{3\Gamma}{2}\left[\frac{\sin\kappa_{jl}}{\kappa_{jl}} + \frac{\cos\kappa_{jl}}{\kappa_{jl}^2} - \frac{\sin\kappa_{jl}}{\kappa_{jl}^3} \right] \tag{S8}$$

It is clear from the form of Eqs. (S4) and (S7) that the dynamics of the internal level $m_J = 0$ is disconnected from the other two. We will consider thus only the dynamics on the subspace formed by the states $m_J = \pm 1$.

II. EWALD SUMMATION

A. General notions

We briefly review the Ewald summation technique [4, 5] introduced originally to cope with the evaluation of the electrostatic potential energy of a gas of electrons interacting through the Coulomb force. Here we wish to evaluate the discrete sum in Eq. (12) of the main text. Considering two-dimensional lattices with unit cell defined by two lattice vectors $(\mathbf{a}_1, \mathbf{a}_2)$, a vector $\mathbf{r}$ connecting two atoms α and β can be written as

$$\mathbf{r} = \boldsymbol{\tau}_{\alpha\beta} + \mathbf{T}, \tag{S9}$$

where $\mathbf{T} = (m\mathbf{a}_1, n\mathbf{a}_2),\ m, n \in \mathbb{Z}$ is the lattice translation vector, $\boldsymbol{\tau}_{\alpha\beta} = \boldsymbol{\tau}_\beta - \boldsymbol{\tau}_\alpha$ and $\boldsymbol{\tau}_\alpha$ denotes the position of the α-th atom in the unit cell. We also define the reciprocal lattice vectors in the usual way as $\mathbf{G} = (m\mathbf{b}_1, n\mathbf{b}_2),\ m, n \in \mathbb{Z}$, where $\mathbf{b}_j,\ j = 1, 2$ are the primitive reciprocal lattice vectors.

Let us consider an algebraically decaying function of the atomic separation $v(\mathbf{r})$ and say we want to evaluate the sum

$$V(\mathbf{k}) = \sum_{\mathbf{r}\neq 0} \mathrm{e}^{i\mathbf{k}\mathbf{r}} v(\mathbf{r}). \tag{S10}$$

Ewald's trick consists of separating the contributions of v to the sum to the short (S) and long (L) ranged part by introducing a regulating function ξ through the identity

$$1 = {}^{S}\xi(r) + {}^{L}\xi(r), \tag{S11}$$

so that

$$V(\mathbf{k}) = {}^{S}V(\mathbf{k}) + {}^{L}V(\mathbf{k}) - {}^{\mathrm{self}}V(\mathbf{k}), \tag{S12}$$

where

$$ {}^{S}V(\mathbf{k}) = \sum_{\mathbf{r}\neq 0} \mathrm{e}^{i\mathbf{k}\mathbf{r}} {}^{S}\xi(r) v(\mathbf{r}) \tag{S13a}$$

$$ {}^{L}V(\mathbf{k}) = \sum_{\mathbf{r}} \mathrm{e}^{i\mathbf{k}\mathbf{r}} {}^{L}\xi(r) v(\mathbf{r}) \tag{S13b}$$

$$ {}^{\mathrm{self}}V(\mathbf{k}) = \lim_{r\to 0} \mathrm{e}^{i\mathbf{k}\mathbf{r}} {}^{L}\xi(r) v(\mathbf{r}). \tag{S13c}$$

The function ξ is chosen such that ${}^{S}\xi(r)v(\mathbf{r})$ decays exponentially fast as $r \to \infty$ and (S13c) is finite. Due to the fast decay of ${}^{S}\xi$, the short-range part can be readily obtained by evaluating the sum in (S13a) in real space. We are thus left with the evaluation of (S13b).

We proceed as follows. Using (S9), (S13b) becomes

$$\begin{aligned}
{}^{L}V(\mathbf{k}) &= \sum_{\alpha,\beta\in\text{unit cell}} \sum_{\mathbf{T}} \mathrm{e}^{i\mathbf{k}(\boldsymbol{\tau}_{\alpha\beta}+\mathbf{T})} {}^{L}\xi(|\boldsymbol{\tau}_{\alpha\beta}+\mathbf{T}|) v(\boldsymbol{\tau}_{\alpha\beta}+\mathbf{T}) \\
&= \sum_{\alpha,\beta\in\text{unit cell}} \mathrm{e}^{i\mathbf{k}\boldsymbol{\tau}_{\alpha\beta}} \int \mathrm{d}^2\mathfrak{r} \sum_{\mathbf{T}} \delta^2(\mathfrak{r}-\mathbf{T}) \mathrm{e}^{i\mathbf{k}\mathfrak{r}} {}^{L}\xi(|\boldsymbol{\tau}_{\alpha\beta}+\mathfrak{r}|) v(\boldsymbol{\tau}_{\alpha\beta}+\mathfrak{r}) \\
&= \sum_{\mathbf{G}} \sum_{\alpha,\beta\in\text{unit cell}} \mathrm{e}^{i\mathbf{k}\boldsymbol{\tau}_{\alpha\beta}} \int \mathrm{d}^2\mathfrak{r} \mathrm{e}^{i\mathbf{k}+\mathbf{G}\mathfrak{r}} {}^{L}\xi(|\boldsymbol{\tau}_{\alpha\beta}+\mathfrak{r}|) v(\boldsymbol{\tau}_{\alpha\beta}+\mathfrak{r}) \\
&= \sum_{\mathbf{G}} \sum_{\alpha,\beta\in\text{unit cell}} \mathrm{e}^{-i\mathbf{G}\boldsymbol{\tau}_{\alpha\beta}} \int \mathrm{d}^2 r \mathrm{e}^{i\tilde{\mathbf{G}}\mathbf{r}} {}^{L}\xi(r) v(\mathbf{r}),
\end{aligned} \tag{S14}$$

where we in the third line we have used the identity (normalizing the volume of the unit cell to 1)

$$\sum_{\mathbf{T}} \delta^2(\mathfrak{r}-\mathbf{T}) = \sum_{\mathbf{G}} \mathrm{e}^{i\mathbf{G}\mathbf{r}} \tag{S15}$$

and in the last line we made a substitution of variables $\mathbf{r} = \boldsymbol{\tau}_{\alpha\beta} + \mathfrak{r}$ and defined $\widetilde{\mathbf{G}} = \mathbf{k} + \mathbf{G}$.

Next, due to the form of Eqs. (4), (6), and (7) in the main text, we consider the following functions v

$$ {}_{1,n}v(\mathbf{r}) = \frac{\cos\kappa r}{\kappa r}\mathrm{e}^{in\phi(\mathbf{r})} \tag{S16a} $$

$$ {}_{2,n}v(\mathbf{r}) = \frac{\sin\kappa r}{(\kappa r)^2}\mathrm{e}^{in\phi(\mathbf{r})} \tag{S16b} $$

$$ {}_{3,n}v(\mathbf{r}) = \frac{\cos\kappa r}{(\kappa r)^3}\mathrm{e}^{in\phi(\mathbf{r})}, \tag{S16c} $$

where $n = 0, 2$ and $\kappa = 2\pi/\lambda$.

B. Analytical approach to the $1/r$ term: the divergence

We start with the evaluation of the integral in (S14) with the function ${}_{1,n}v(\mathbf{r})$

$$ \begin{aligned} {}_{1,n}\mathfrak{V} &\equiv \int \mathrm{d}^2 r \mathrm{e}^{i\widetilde{\mathbf{G}}\mathbf{r}} {}^L\xi(r)\,{}_{1,n}v(\mathbf{r}) \\ &= \kappa^{-1}\int_0^\infty \mathrm{d}r\left(1-\mathrm{e}^{-\gamma r}\right)\cos(\kappa r)\int_0^{2\pi}\mathrm{d}\varphi \mathrm{e}^{i(\widetilde{G}r\cos(\varphi-\eta)+n\phi(\mathbf{r}))} \\ &= \kappa^{-1}\int_0^\infty \mathrm{d}r\left(1-\mathrm{e}^{-\gamma r}\right)\cos(\kappa r)J_n(\widetilde{G}r), \end{aligned} \tag{S17} $$

where we have chosen ${}^L\xi(r) = 1-\mathrm{e}^{-\gamma r}$, $\gamma > 0$ is an arbitrary control parameter, η is the polar angle of $\widetilde{\mathbf{G}}$ and J_n is the n-th Bessel function of the first kind. Next, we split the integration as

$$ {}_{1,n}\mathfrak{V} = {}_{1,n}\mathfrak{V}_0^c + {}_{1,n}\mathfrak{V}_c^\infty, \tag{S18} $$

where

$$ {}_{1,n}\mathfrak{V}_a^b = \kappa^{-1}\int_a^b \mathrm{d}r\left(1-\mathrm{e}^{-\gamma r}\right)\cos(\kappa r)J_n(\widetilde{G}r). \tag{S19} $$

Finally, we substitute the asymptotic expression for the Bessel function (for large $\widetilde{G}r$)

$$ J_n(\widetilde{G}r) \approx \sqrt{\frac{2}{\pi\widetilde{G}}}\frac{1}{\sqrt{r}}\cos\left(\widetilde{G}r-\phi_n\right), \tag{S20} $$

where $\phi_n = \frac{\pi}{4}(2n+1)$, to ${}_{1,n}\mathfrak{V}_c^\infty$ so that

$$ {}_{1,n}\mathfrak{V}_c^\infty \approx I_0^\infty - I_0^c, \tag{S21} $$

where

$$ I_a^b = \frac{1}{\kappa}\sqrt{\frac{2}{\pi\widetilde{G}}}\int_c^d \mathrm{d}r\frac{1-\mathrm{e}^{-\gamma r}}{\sqrt{r}}\cos(\kappa r)\cos(\widetilde{G}r-\phi_n). \tag{S22} $$

Importantly, we note, that only the term I_0^∞ can give rise a the divergence in (S12), which we now analyze in detail. Substituting the identity

$$ \frac{1}{\sqrt{r}} = \frac{1}{\sqrt{\pi}}\int_0^\infty \mathrm{d}t t^{-\frac{1}{2}}\mathrm{e}^{-tr} \tag{S23} $$

and using

$$ \cos a\cos b = \frac{1}{2}\left[\cos(a+b)+\cos(a-b)\right] \tag{S24} $$

we get

$$ \kappa\pi\sqrt{\frac{\widetilde{G}}{2}}I_0^\infty = \int_0^\infty \mathrm{d}t t^{-\frac{1}{2}}\int_0^\infty \mathrm{d}r\left(1-\mathrm{e}^{-\gamma r}\right)\mathrm{e}^{-tr}\left[\cos((\widetilde{G}+\kappa)r-\phi_n)+\cos((\widetilde{G}-\kappa)r-\phi_n)\right]. \tag{S25} $$

This amounts to evaluation of the integral

$$\begin{aligned} II &= \int_0^\infty \mathrm{d}t t^{-\frac{1}{2}} \int_0^\infty \mathrm{d}r \left(1 - \mathrm{e}^{-\gamma r}\right) \mathrm{e}^{-tr} \cos(\mathcal{G}r - \phi_n) \\ &= \frac{\mathrm{e}^{-i\phi_n}}{2} \int_0^\infty \mathrm{d}t \frac{1}{\sqrt{t}} \int_0^\infty \mathrm{d}r \left[\mathrm{e}^{-tr} - \mathrm{e}^{-(t+\gamma)r}\right] \mathrm{e}^{i\mathcal{G}r} + \text{c.c.} \\ &= \frac{\mathrm{e}^{-i\phi_n}}{2} \int_0^\infty \mathrm{d}t \frac{1}{\sqrt{t}} \left(\frac{1}{t - i\mathcal{G}} - \frac{1}{t + \gamma - i\mathcal{G}}\right) + \text{c.c.}, \end{aligned} \tag{S26}$$

where $\mathcal{G} = \widetilde{G} \pm \kappa$. The final integration in (S26) can be done by methods of contour integration along the contour depicted in Fig. S1, i.e.

$$\oint_C = \int_{C_1} + \int_R + \int_{C_2} + \int_\epsilon. \tag{S27}$$

Using the property of the branch cut, the integration along C_2 becomes

$$\begin{aligned} \int_{C_2} &= \int_R^\epsilon \mathrm{d}z \frac{1}{\sqrt{z}} \left(\frac{1}{z - z_0} - \frac{1}{z - z_1}\right) \\ &= \int_R^\epsilon \mathrm{d}z \frac{1}{\mathrm{e}^{\frac{1}{2}(\log|z| + i2\pi)}} \left(\frac{1}{z - z_0} - \frac{1}{z - z_1}\right) \\ &= \int_R^\epsilon \mathrm{d}z \frac{1}{-\sqrt{z}} \left(\frac{1}{z - z_0} - \frac{1}{z - z_1}\right) \\ &= \int_\epsilon^R \mathrm{d}z \frac{1}{\sqrt{z}} \left(\frac{1}{z - z_0} - \frac{1}{z - z_1}\right). \end{aligned} \tag{S28}$$

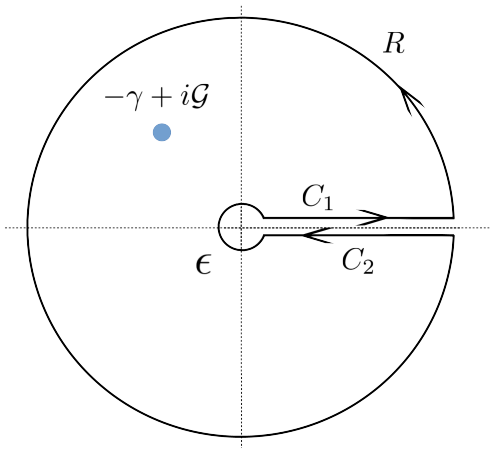

FIG. S1. Integration contour

Omitting the c.c. term, we express the leftmost part of (S26) as

$$II_- = \frac{\mathrm{e}^{-i\phi_n}}{2} \int_0^\infty \mathrm{d}z \frac{1}{\sqrt{z}} \left(\frac{1}{z - i\mathcal{G}} - \frac{1}{z + \gamma - i\mathcal{G}}\right) \tag{S29}$$

$$= \int_0^\infty \mathrm{d}z g(z) = \int_0^\infty \mathrm{d}z \frac{f(z)}{z - z_0} - \frac{f(z)}{z - z_1}. \tag{S30}$$

It can be immediately seen, that $\int_R \to 0$ since $g(z) \to R^{-\frac{3}{2}}$ in the limit of large $|z|$. Next, since $\gamma > 0$, assuming $\mathcal{G} \neq 0$ and substituting $z = \epsilon \mathrm{e}^{i\varphi}$, we get from the estimation lemma

$$\left|\int_\epsilon\right| \leq |g(z)| 2\pi\epsilon \propto 2\pi \frac{\epsilon}{\sqrt{\epsilon}} \xrightarrow{\epsilon \to 0^+} 0. \tag{S31}$$

We are thus left with

$$II_- = \frac{1}{2}\oint_C = i\pi\left(f(z_0) - f(z_1)\right) \tag{S32}$$
$$= i\pi\frac{\mathrm{e}^{-i\phi_n}}{2}\left[\frac{1}{\sqrt{i\mathcal{G}}} - \frac{1}{\sqrt{-\gamma+i\mathcal{G}}}\right],$$

where we have defined the function f and the poles

$$f(z) = \frac{\mathrm{e}^{-i\phi_n}}{2}\frac{1}{\sqrt{z}}$$
$$z_0 = i\mathcal{G}$$
$$z_1 = -\gamma + i\mathcal{G}. \tag{S33}$$

Plugging (S32) back to (S26) and evaluating the complex conjugated term we get

$$\begin{aligned}\frac{2}{\pi}II &= i\mathrm{e}^{-i\phi_n}\left[\frac{1}{\sqrt{i\mathcal{G}}} - \frac{1}{\sqrt{-\gamma+i\mathcal{G}}}\right] + \text{c.c}\\ &= i\cos(\phi_n)\left[\frac{1}{\sqrt{i\mathcal{G}}} - \frac{1}{\sqrt{-i\mathcal{G}}} + \frac{1}{\sqrt{-\gamma-i\mathcal{G}}} - \frac{1}{\sqrt{-\gamma+i\mathcal{G}}}\right] + \sin(\phi_n)\left[\frac{1}{\sqrt{i\mathcal{G}}} + \frac{1}{\sqrt{-i\mathcal{G}}} - \frac{1}{\sqrt{-\gamma-i\mathcal{G}}} + \frac{1}{\sqrt{-\gamma+i\mathcal{G}}}\right]\\ &= 2\left\{\frac{\cos(\phi_n)\sin[\frac{1}{2}\arg(i\mathcal{G})]}{|\mathcal{G}|^{\frac{1}{2}}} - \frac{\cos(\phi_n)\sin[\frac{1}{2}\arg(\gamma+i\mathcal{G})]}{|\gamma+i\mathcal{G}|^{\frac{1}{2}}} + \frac{\sin(\phi_n)\cos[\frac{1}{2}\arg(i\mathcal{G})]}{|\mathcal{G}|^{\frac{1}{2}}} + \frac{\sin(\phi_n)\cos[\frac{1}{2}\arg(\gamma+i\mathcal{G})]}{|\gamma+i\mathcal{G}|^{\frac{1}{2}}}\right\}\end{aligned} \tag{S34}$$

Next, we note that this result can be further simplified in specific cases: for $\mathcal{G}\in\mathbb{R}$ and $n = 0, 2$ respectively, we get the following options

$$\begin{aligned}&n = 0: \ \phi_0 = \frac{\pi}{4} \to \sin(\frac{\pi}{4}) = \frac{1}{\sqrt{2}}; \quad \cos(\frac{\pi}{4}) = \frac{1}{\sqrt{2}}\\ &n = 2: \ \phi_2 = \frac{5\pi}{4} \to \sin(\frac{5\pi}{4}) = \frac{1}{\sqrt{2}}; \quad \cos(\frac{5\pi}{4}) = -\frac{1}{\sqrt{2}}\\ &\mathcal{G} > 0: \ \arg(i\mathcal{G}) = \frac{\pi}{2} \to \sin(\frac{1}{2}\arg(i\mathcal{G})) = \frac{1}{\sqrt{2}}; \quad \cos(\frac{1}{2}\arg(i\mathcal{G})) = \frac{1}{\sqrt{2}}\\ &\mathcal{G} < 0: \ \arg(i\mathcal{G}) = -\frac{\pi}{2} \to \sin(\frac{1}{2}\arg(i\mathcal{G})) = -\frac{1}{\sqrt{2}}; \quad \cos(\frac{1}{2}\arg(i\mathcal{G})) = \frac{1}{\sqrt{2}}.\end{aligned} \tag{S35}$$

Lets first consider the $n = 0$ case. Using (S35), the relation (S34) simplifies to

$$\begin{aligned}&\mathcal{G} > 0: \ \frac{1}{\pi}II_{n=0}(\mathcal{G}) = \frac{1}{|\mathcal{G}|^{\frac{1}{2}}} - \frac{1}{\sqrt{2}|\gamma+i\mathcal{G}|^{\frac{1}{2}}}\left(\sin(\frac{1}{2}\arg(\gamma+i\mathcal{G})) - \cos(\frac{1}{2}\arg(\gamma+i\mathcal{G}))\right)\\ &\mathcal{G} < 0: \ \frac{1}{\pi}II_{n=0}(\mathcal{G}) = -\frac{1}{\sqrt{2}|\gamma+i\mathcal{G}|^{\frac{1}{2}}}\left(\sin(\frac{1}{2}\arg(\gamma+i\mathcal{G})) - \cos(\frac{1}{2}\arg(\gamma+i\mathcal{G}))\right).\end{aligned} \tag{S36}$$

and similar expression is obtained for $n = 2$. Those results can be combined to a single expression

$$\frac{1}{\pi}II_n(\mathcal{G}) = \frac{(-1)^n}{|\mathcal{G}|^{\frac{1}{2}}}\theta(\mathcal{G}) - \frac{1}{\sqrt{2}|\gamma+i\mathcal{G}|^{\frac{1}{2}}}\left(\sin(\frac{1}{2}\arg(\gamma+i\mathcal{G})) - \cos(\frac{1}{2}\arg(\gamma+i\mathcal{G}))\right), \tag{S37}$$

where θ is the Heaviside step function. Remarkably, the function (S37) is finite in the limit $\mathcal{G}\to 0^-$, but diverges as $\mathcal{G}\to 0^+$, which constitutes the main analytic result of this section.

Remark: The discontinuity and one-sided divergence could be seen already in (S26) by setting $\mathcal{G} = 0$. This would result in the diverging integral in the vicinity of the origin, namely the part $\int_\epsilon \propto \int \mathrm{d}t\frac{1}{t\sqrt{t}}$ in (S27), which, according to the estimation lemma, scales as $\propto \frac{1}{\sqrt{\epsilon}}$.

C. Numerical implementation

In the previous section we have found that (S13a),(S13c) can be evaluated numerically, while (S13b) can be written as

$${}^{L}_{1,n}V(\mathbf{k}) = \sum_{\mathbf{G}}\sum_{\alpha,\beta\in\text{unit cell}}\mathrm{e}^{-i\mathbf{G}\boldsymbol{\tau}_{\alpha\beta}}\left[{}_{1,n}\mathfrak{V}_0^c - I_0^c + I_0^\infty\right]. \tag{S38}$$

Here, the expressions ${}_{1,n}\mathfrak{V}_0^c$ and I_0^c are finite and can by obtained numerically. In principle similar decomposition can be obtained when considering the functions (S16b),(S16c), however we found it more convenient to evaluate the corresponding element (S10) by direct summation in real space.

The final subtlety is related to the fact, that for ${}^L\xi = 1 - \mathrm{e}^{-\gamma r}$ the self-interaction term (S13c) is not defined for ${}_{1,n=2}v$ as it depends on the direction in which the origin is approached (which is due to the dependence of ${}_{1,n=2}v$ on the polar angle of $\mathbf{r}$). This problem can be circumvented by considering ${}^L\xi = 1 - \mathrm{e}^{-\gamma r^2}$ instead in which case the self-interaction term vanishes. Here, it is still possible to evaluate the integral in (S22) symbolically, which we then use in (S38).

In (S38) the tuning parameters γ, c are chosen such that the approximations used [Eq. (S20)] are well satisfied.

III. FINITE-SIZE EFFECTS AND THE BULK-BOUNDARY RELATION

A. Characterization of topological properties in finite-size systems

We investigate here the properties of edge states and the related excitation propagation in finite systems in order to better understand the impact of the limited spatial extent of the system on the resulting topological characteristics.

In Figs. 2(a) and (b) of the main text we show the phase diagrams (the bulk Chern number C, Eq. (13), as a function of the TRS breaking parameters) for the SL and HL geometries. These are obtained from the eigenstates obtained by the method of Ewald summation described in Sec. II C of this Supplemental Material. We refer to the results obtained in this way as the thermodynamic limit. Note, that the change in C is always connected to the closing of the corresponding gap.

As mentioned in the main text, the bulk Chern number is formally well defined on differentiable manifolds and evaluated in the thermodynamic limit. While there is a one-sided divergence in the spectrum appearing as a consequence of the far-field terms of the interaction, the bulk Chern number can be still obtained by avoiding the divergence points in the numerical calculation (see also [6] for a related discussion of the divergences in systems with long-range potentials). The divergences get effectively regularized when considering finite-size lattices. We define the finite-size analogue of the Chern number C_N as the discretized version of Eq. (12) evaluated on a finite system with N atoms. We implement the periodic boundary conditions in this finite system by assuming that each atom interacts through the *same* potential $\bar{V}_{\mathbf{r}}$, i.e., $\sum_{j\neq l=1}^{N} e^{i\mathbf{k}\cdot\mathbf{r}_{jl}}\overline{V}_{jl} = \sum_{\mathbf{r}\neq 0} e^{i\mathbf{k}\cdot\mathbf{r}}\overline{V}_{\mathbf{r}}$.

Similarly to the results obtained in the thermodynamic limit, we observe that a transition between different Chern numbers C_N results from a closing of the corresponding gap. However, for finite-size systems, the value of the TRS-breaking parameter Δ^C at which the gap closing appears varies with the system size evolving towards the result obtained in the thermodynamic limit as the system size increases. This is demonstrated in Fig. S2(a) for an HL, where we show Δ^C/Γ as a function of N for the transition occurring at $\Delta/\Gamma = -6$ in the thermodynamic limit [see Fig. S2(b)]. Depending on the parameter regime considered, the system size can have a dramatic influence on the system properties, namely a series of transitions between different C_N as the system size is varied [see Fig. S2(c) for $\Delta/\Gamma = -5$]. We note that such dependence on the system size is not observed when considering the near-field limit resulting in the potential decaying as $1/r^3$, see Fig. 3 in [7].

B. Edge state profiles and the bulk-boundary relationship

In this section we investigate in some detail the mechanism underlying the apparent breaking of the bulk-boundary relationship observed in the case of HL, namely the fact that the edge states expected to exist in the second gap are not robust with respect to local perturbations. To this end we plot the band structure of an infinite strip with finite extent in the y-direction with $N_y = 20$ atoms in Fig. S3(a). Here, if we label the eigenenergies and the corresponding single particle eigenstates as $E(k_x, n)$ and $|\psi_{k_x,n}(y)\rangle$, where $n = \{1, \ldots, 4N_y\}$, then $n_j = \{jN_y, jN_y + 1\}$ are the modes crossing the first ($j = 1$) and the second ($j = 2$) gap, respectively. The black boxes in Fig. S3(a) denote the modes (i.e. fixing n_j and k_x) which have maximal weight (from all the modes lying in the gap) on either edge of the lattice (edge 1, red datapoints or edge 2, blue datapoints). The profiles of the states $|\psi_{k_x,n_j}(\tilde{y})|^2$ of the maximal-weight-on-the-edge modes as a function of $\tilde{y}$ are plotted in Fig. S3(c) (here $\tilde{y}$ simply denotes the number of the site in the y-direction rather than the real-space position). It is apparent from Fig. S3(c) that the modes from the second gap have approximately two orders of magnitude larger weight in the bulk than the modes from the first gap. For comparison we show in Figs. S3(b) and (d) the case $N_y = 80$, and observe that the situation remains qualitatively the same. Furthermore, we note that the modes crossing the first (second) gap have $|k_x| > \kappa$ ($|k_x| < \kappa$), with $\kappa = 2\pi/\lambda$.

The increased overlap of the modes crossing the second gap and the fact that they lie effectively inside the divergence circle [8] have important consequences for the closed and open dynamics respectively. In the absence of dissipation,

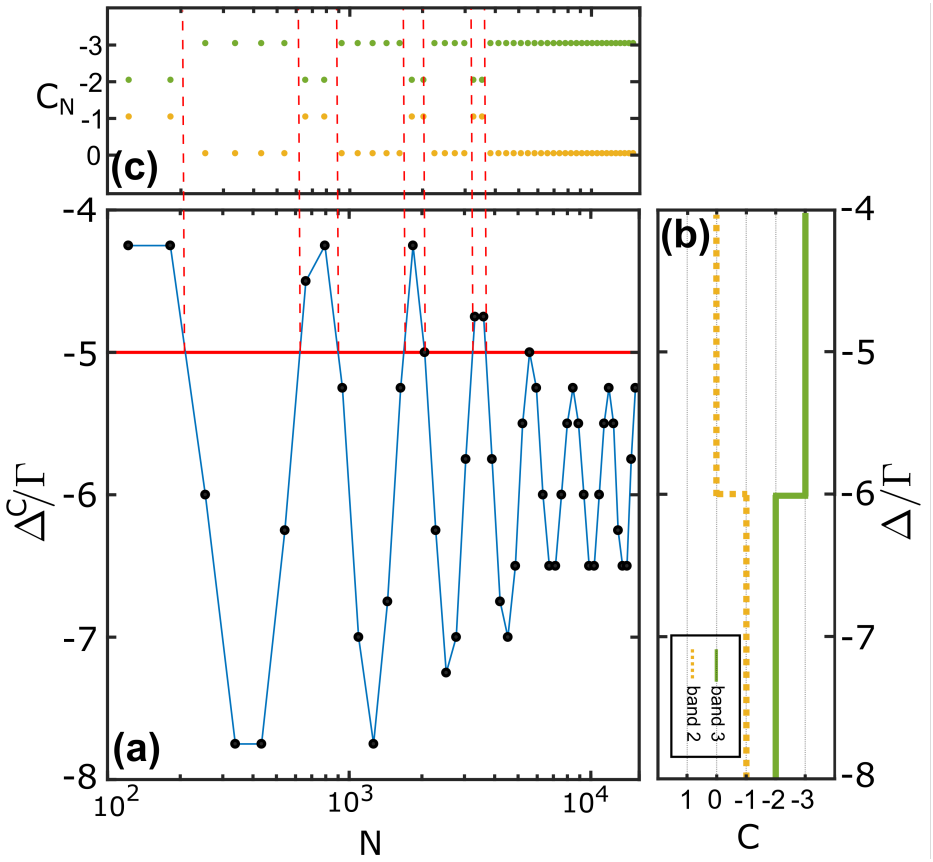

FIG. S2. **(a):** Value of Δ/Γ at which the gap between the second and third band closes, $\Delta^{\mathrm{C}}/\Gamma$, as a function of the system size N. **(b):** Chern number C of the same two bands when calculated in the thermodynamic limit. **(c):** Chern number C_N as a function of the system size N at $\Delta/\Gamma = -5$ [red solid line in (a)], with the red dashed lines indicating a closing of the gap, which coincides with a change in C_N.

we interpret the inhibition of excitation transport due to the presence of lattice defects observed in the fourth panel of Fig. 3(b) to be a consequence of the increased overlap of the excited mode with the bulk ones resulting in an enhanced proliferation of the excitation into the bulk and thus inhibiting the transport along the edge. In the presence of dissipation, it is extensively discussed in a work closely related to ours [9], that the modes with $|k| < \kappa$ are superradiant (as opposed to the subradiant ones with $|k| > \kappa$), which has again for a consequence an inhibition of excitation propagation (we note that the separation between the sub and superradiant modes occurring at $|k| = \kappa$ is a direct consequence of the $1/r$ long-range part of the potential [9]).

So far we were only concerned by modes with maximum weight on the edges of the lattice. To complete our discussion, in Figs. S3(e) and (f) we plot the spatial profiles of the k_x-modes of the spectral branches indicated by arrows in Fig. S3(a). Specifically, for the branch lying in the first gap, we plot all $k_x < 0$ and for the branch in the second gap $k_x \geq 0$. The green (grey) lines correspond to modes with $|k_x| > \kappa$ ($|k_x| < \kappa$). The spatial profiles of the modes with highest weight on edge 1 are highlighted in red [and indicated by arrows between Figs. S3(c) and S3(e) and (f)]. The thick green (thick grey) line in Fig. S3(e) [Fig. S3(f)] denotes the energetically degenerate mode with equal support on both edges corresponding to $k_x b/\pi = -1$ ($k_x b/\pi = 0$). In Fig. S3(e) the grey lines correspond to the bulk modes, which is also the case for most of the green lines in Fig. S3(f). The main message of these figures is that small (increased) overlap with the bulk modes is not a special property of the modes with maximal weight on the edge, but a generic feature of the modes lying well within the first (second) gap.

[1] R. H. Lehmberg, Phys. Rev. A **2**, 883 (1970).
[2] G. S. Agarwal, Phys. Rev. A **2**, 2038 (1970).
[3] D. F. V. James, Phys. Rev. A **47**, 1336 (1993).

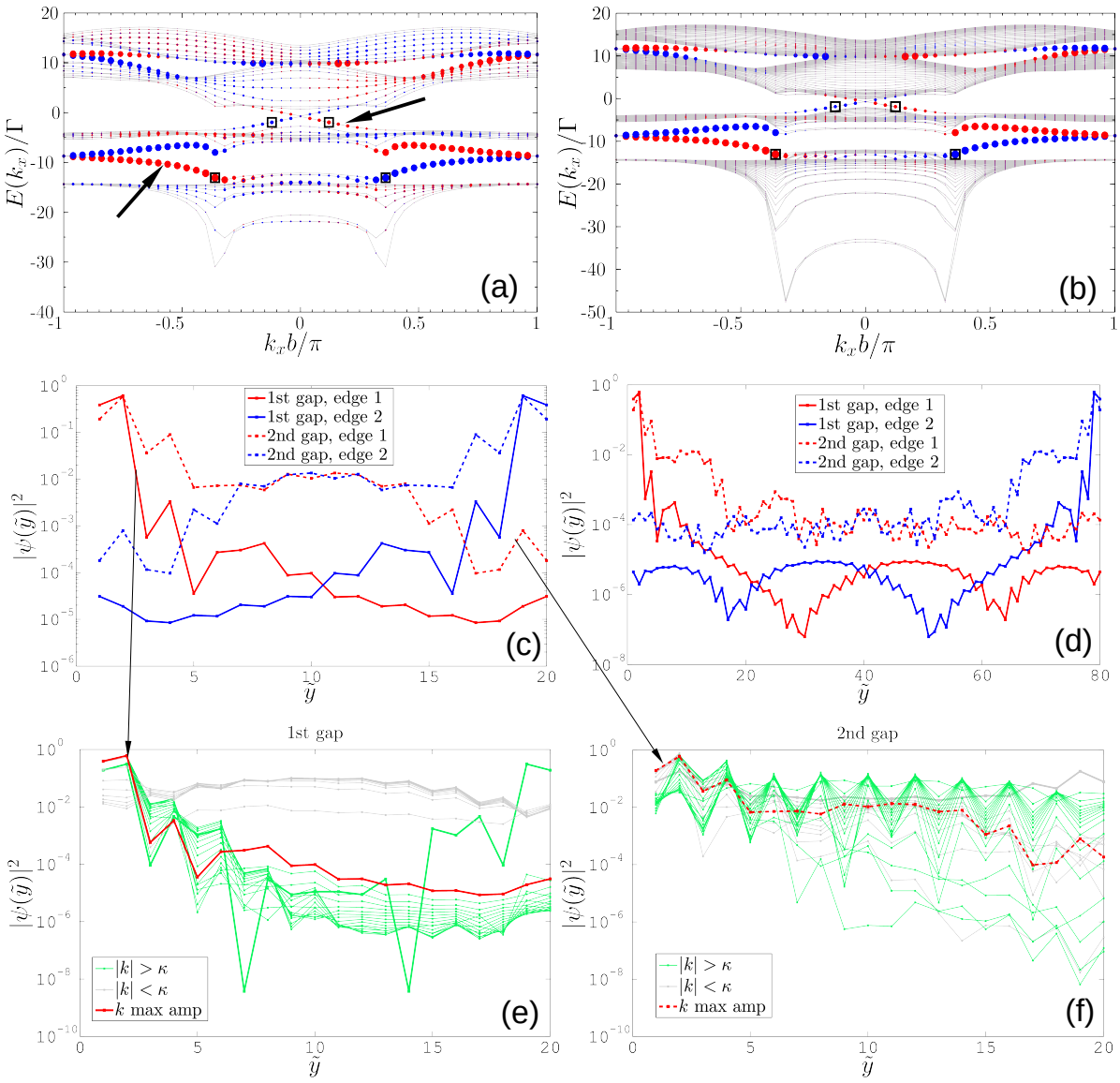

FIG. S3. Band structure of the HL in the infinite strip geometry with zigzag boundaries and finite extent in the y-direction for $N_y = 20$ **(a)** and $N_y = 80$ **(b)**. Here the weight of the given mode at one (the other) boundary is depicted as red (blue) circles with the size of the circle proportional to the amplitude. The black boxes highlight the k-modes with maximal amplitude in the first and second gaps respectively. **(c)** Spatial profiles of the k-modes with maximal amplitude on the boundary, where solid (dashed) lines correspond to the modes in the first (second) gap respectively and red (blue) to either edge. **(d)** The same as (c) for $N_y = 80$. Edge state profiles across the strip for the first **(e)** and second **(f)** gap for $N_y = 20$ and for the branches indicated by arrows in (a). See text for details.

[4] L. Bonsall and A. A. Maradudin, Phys. Rev. B **15**, 1959 (1977).
[5] L. Kantorovich, *Quantum theory of the solid state: an introduction*, Vol. 136 (Springer Science & Business Media, 2004).
[6] L. Lepori and L. DellAnna, preprint , arXiv:1612.08155 (2017).
[7] D. Peter, N. Y. Yao, N. Lang, S. D. Huber, M. D. Lukin, and H. P. Büchler, Phys. Rev. A **91**, 053617 (2015).
[8] Although there is no divergence in the spectrum in the strip geometry, which is recovered in the $N_y \to \infty$ limit, its influence is still clearly visible.
[9] A. Asenjo-Garcia, M. Moreno-Cardoner, A. Albrecht, H. J. Kimble, and D. E. Chang, Phys. Rev. X **7**, 031024 (2017).